Building the inhomogeneous finite element model by the data of computed tomography

Article · January 2018

DOI: 10.15593/RJBiomeh/2018.3.05

9 authors, including:

O.A. Sachenkov
Kazan Federal University
68 PUBLICATIONS **426** CITATIONS
SEE PROFILE

Oleg Gerasimov
Kazan Federal University
22 PUBLICATIONS **116** CITATIONS
SEE PROFILE

Viktoriya V. Yaikova
5 PUBLICATIONS **24** CITATIONS
SEE PROFILE

ISSN 1812-5123. Russian Journal of Biomechanics. 2018. V. 22, № 3: 290–302

DOI: 10.15593/RJBiomeh/2018.3.05

Russian Journal of Biomechanics
www.biomech.ru

BUILDING THE INHOMOGENEOUS FINITE ELEMENT MODEL BY THE DATA OF COMPUTED TOMOGRAPHY

O.A. Sachenkov[1,4], O.V. Gerasimov[1], E.V. Koroleva[1], D.A. Mukhin [1], V.V. Yaikova[1], I.F. Akhtyamov[2], F.V. Shakirova[3], D.A. Korobeynikova[2], H.Ch. Khan[3]

[1] Institute of Mathematics and Mechanics, Kazan Federal University, 18 Kremlevskaya Str., Kazan, 420008, Russia, e-mail: 4works@bk.ru
[2] Kazan State Medical University, 49 Butlerova Str., Kazan, 420012, Russia, e-mail: yalta60@mail.ru
[3] Kazan State Academy of Veterinary Medicine, 35 Sibirskiy Trakt, Kazan, 420029, Russia, e-mail: shakirova-fv@yandex.ru
[4] Kazan National Research Technical University named after A.N. Tupolev, 10 Karl Marx Str., Kazan, 420111, Russia.

Abstract. The aim of the work is to reveal a methodology for constructing a finite element model by tomography data. To evaluate the model, calculations of the femur were carried out. The relevance of this study is confirmed by the effect of the distribution of the mechanical properties of the bone on stress-strain state and the need for individualizing the approach to modeling. Numerical studies were performed using the finite element method in the Ansys software, computer tomography data processing was carried out in the Avizo software. The problem of a linear inhomogeneous elastic body was considered. Power functions of the optical density were used to determine the Young's modulus and the limiting voltage, in turn, the optical density was determined from linear relations depending on the Hounsfield numbers. For finite element model, the mechanical properties of the material were distributed for each element according to the tomography data. After solving the problem of the stress-strain state, at each node a factor of safety was determined adjusted for the properties of the material from the tomography data. Inhomogeneous and homogeneous models with average properties were built. Calculations for both models were performed. Numerical results clearly illustrate significant differences in the results of the stress-strain state of the inhomogeneous and homogeneous models of the organ. Inhomogeneous model allows us to evaluate the local strength of bone tissue taking into account individual characteristics.

Key words: mathematical modeling, inhomogeneous media, computed tomography.

Oskar A. Sachenkov, Ph.D., Researcher, Department of Theoretical Mechanics, Kazan
Oleg V. Gerasimov, Student, Department of Theoretical Mechanics, Kazan
Yelizaveta V. Koroleva, Student, Department of Theoretical Mechanics, Kazan
Dmitriy A. Mukhin, Student, Department of Theoretical Mechanics, Kazan
Viktoriya V. Yaikova, Student, Department of Theoretical Mechanics, Kazan
Ildar F. Akhtyamov, Ph.D., Head of Department of Traumatology, Orthopedics and Surgery of Extreme Conditions, Kazan
Faina V. Shakirova, Ph.D., Professor, Department of Surgery, Obstetrics and Pathology of Small Animals, Kazan
Darya A. Korobeynikova, Postgraduate Student, Department of Surgery, Obstetrics and Pathology of Small Animals, Kazan
Khan Khao Chzhi, Postgraduate Student, Department of Traumatology, Orthopedics and Surgery of Extreme Conditions, Kazan

INTRODUCTION

Bone tissue has inhomogeneous mechanical properties, because of its adaptive properties [3, 8, 32, 35, 36]. Decreased physical activity [11, 31], physiological [12, 13] or age-related features can lead to local loss of bone strength. In clinical practice, this can lead to a discrepancy between the actual behavior of the organ and the expected (simulated) results of surgical intervention. In orthopedics and traumatology, many studies are aimed at improving the methods of surgical intervention [22, 25, 26], optimizing the use of rod devices [2, 4, 6-10], but in practice, due to the complexity of predicting the behavior of bone tissue material [19, 27-29], many decisions about the tactics of the operation have to be made by the surgeon on the spot. Take into account the above-mentioned facts, it can be conclude that it is important to evaluate the mechanical properties of an organ, not in an integral sense, but in a distributed sense. Modern approaches to numerical modelling allow us to solve problems for complex areas [5, 14, 16, 17, 20, 23, 34], together with the development of computer tomography, and this allows to adjudicate the internal structure of the organ, the task of individualization in modelling organs from bone tissue can provide useful information in the preoperative period.

The aim of the study is to construct a finite element model that allows us to take into account the distribution of mechanical properties (Young's modulus and ultimate strength) from computed tomography data and the determination of the stress-strain behavior for the constructed model.

MATERIALS AND METHODS

Formulation of a problem

Assumptions: Authors assume that the material is isotropic and inhomogeneous. Moreover, from the assumption of a connection between physical density and mechanical characteristics, we will use the optical density to calculate the Young's modulus and the ultimate stresses.

Mathematical model

The calculation area includes some inhomogeneous body. Authors denote it by V, and for ∂V the boundary of this set (free surface). The mechanical behavior of a system occupying a region V in R^3 with a boundary ∂V in the framework of the linear theory of elasticity is described by the following system of equations:

$$\nabla \cdot \tilde{\sigma} = 0, \ \forall x \in V, \tag{1}$$

$$\tilde{\varepsilon} = \frac{1}{2}(\nabla \vec{u} + (\nabla \vec{u})^T), \ \forall x \in \bar{V}, \tag{2}$$

$$\tilde{\sigma} = \varphi(\vec{x}) \cdot \tilde{\tilde{E}} : \tilde{\varepsilon} \ , \ \forall x \in \bar{V}, \tag{3}$$

where $V = V \cup \partial V$, $\tilde{\sigma}$ is stress tensor; $\tilde{\varepsilon}$ is tensor of elastic deformation; $\vec{u}$ is displacement vector; $\tilde{\tilde{E}}$ is tensor of elastic properties, $\varphi(\vec{x})$ is some function that determines the inhomogeneity of the medium.

Moreover, suppose that the ultimate stresses also depend on the spatial coordinate:

$$[\sigma] = [\sigma(\vec{x})], \quad \forall \vec{x} \in V^{\circ}. \tag{4}$$

Then, to estimate the stress-strain body, we introduce the factor of safety defined by the formula:

$$k(\vec{x}) = \frac{\sigma_{VM}(\vec{x})}{[\sigma(\vec{x})]}, \quad \forall \vec{x} \in V^{\circ}, \tag{5}$$

where $\sigma_{VM}(\vec{x})$ is von Mises stress at a given point. In this case, the key role will be played by the zones where the factor of safety (5) above unity.

To build models of organs from bone tissue, it is proposed to use computer tomography data, in which case the computer tomography value $CT(\vec{x})$ can be compared for each point $\vec{x} \in V^{\circ}$. For the convenience of using such data, it is customary to normalize them (Hounsfield scale):

$$\#CT(\vec{x}) = 10^3 \frac{CT(\vec{x}) - CT_w}{CT_w - CT_a}, \tag{6}$$

where CT_w, CT_a are the linear attenuation coefficients for water and air, respectively.

It is known from a wide range of studies [1, 3, 15, 18, 24, 30] that there is a relation between the Hounsfield units and the optical density, elastic constants, and ultimate stress. In general form, these dependences can be written in the following form [18, 24, 30]:

$$\rho = a_\rho + b_\rho \cdot \#\mathrm{CT}, \tag{7}$$

$$E = a_E \rho^{b_E}, \tag{8}$$

$$[\sigma] = a_\sigma \rho^{b_\sigma}, \tag{9}$$

here the coefficients *a* and *b* with the corresponding indices are determined from the experiment and can vary depending on the type of bone tissue or organ.

Numerical solution of the problem

The numerical realization was carried out on the basis of the finite element method. The basic idea is to build up the relationship between the finite element mesh and computer tomography data. To do this, it is necessary on a discretized set, which is a set of node data (their coordinates) and elements (node numbers forming an element), to determine the attenuation coefficients at the nodes.

$$Nd_i = Nd(\vec{x}), \quad \forall \vec{x} \in V^{\circ}{}_D, \ i = 1, N_{node}, \tag{10}$$

$$El_p = El(N_i, N_j, N_k, N_l), \ p = 1, N_{elem}, \tag{11}$$

где $V^{\circ}{}_D$ is the finite element volume V° discretization, $Nd_i, Nd(\vec{x})$ are node number and its coordinates, El_p, El are element number and the node numbers forming it, N_{node}, N_{elem} are number of nodes and elements, respectively.

Further, averaging of the mechanical characteristics for each element is performed, this averaging allows us, in an elastic formulation, to use classical finite elements. To

determine the factor of safety (5), an array of ultimate stress is created, which in dimension coincides with the number of nodes in the mesh. For the processing of tomography data, the software product Avizo was used, for finite element modelling Ansys software was used.

In finite element modelling of the stress-strain state of the organ, four nodal finite element with a linear approximation (solid186) was used. In the element average value of computer tomography data was used. The arithmetic mean was used, which imposes conditions on the shape of the finite element (uniformity of three linear dimensions of the element).

Expressions (7)-(9) can be expressed directly in terms of the Hounsfield scale:

$$E = \tilde{a}_E \cdot \#CT^{\tilde{b}_E}, \tag{12}$$

$$[\sigma] = \tilde{a}_\sigma \cdot \#CT^{\tilde{b}_\sigma}. \tag{13}$$

The used values of the coefficients in the expressions (12)-(13) are given in Table 1. [18, 21, 24, 30].

Table 1

Parameters values

Coefficient	$\tilde{a}$	$\tilde{b}$
Young's modulus E	$46 \cdot 10^3$	2
Ultimate stress σ	60	1.82

For the finite element model, the relationships for determining the factor of safety (5) can be rewritten as:

$$k(Nd_i) = \frac{\sigma_{VM}(Nd_i)}{[\sigma(Nd_i)]}, \quad i = 1, N_{node}. \tag{14}$$

The analysis of stress-strain behavior of the organ will be based on the data of the factor of safety (14).

Model problem

For calculations, the computer tomographydata of femur was used (see Fig. 1, *a*). The following problems were studied: 1) uniaxial compression, 2) bending, and 3) mutual bending with compression. Forces shown in Table 2. To assess the significance of the proposed approach, two models were considered: the first inhomogeneous - the stress-strain behavior is determined by the described method, the second homogeneous - the stress-strain behavior problem is solved for some averaging of the mechanical properties throughout the volume: E = 32 GPa, σ = 48 MPa.

Table 2

Forces values

Calculated case	F_1, N	F_2, N
1	20	0
2	0	200
3	20	200

A femoral sample was scanned on a Vatech PaX-I 3D computer tomograph. The data were processed in the Avizo software package. The threshold of the exterior was determined by the Otsu method, the processing technique is described in more detail in [33]. Further, for a set of points related to the organ, a surface mesh was constructed and then a volume mesh was built. To satisfy the uniformity of the dimensions of the elements, a fairly fine mesh was constructed (about $14 \cdot 10^4$ nodes and $7 \cdot 10^5$ elements).

Data of the mesh and the computer tomography data in the nodes were exported to a file and then the file was loaded into the Ansys software. In Ansys a distribution of averaged (by element) mechanical characteristics was carried out, kinematic and static boundary conditions were applied, a solution and a calculation of the factor of safety (14) were made. In the calculations, the diaphyseal portion of the femur was examined (see Fig. 1, *b*). Fig. 1, *c* shows the scheme of the boundary conditions: the loading force was applied to the cross section *AD*, all displacement of the nodes were fixed on the cross-section *BC*, the forces are given in Table 2. Further, in the Ansys software complex, the stress-strain behavior problem was solved and the reserve factors were calculated by the formula (12).

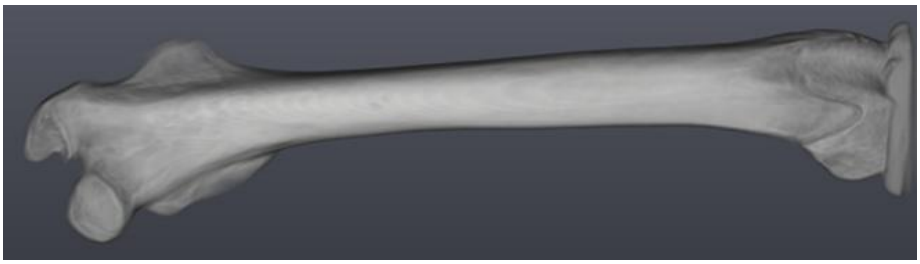

a

b

c

Fig. 1. The sample: *a* is tomography of the femur, *b* is diaphyseal portion of the femur, *c* is the calculation scheme

RESULTS AND DISCUSSION

The finite element mesh was loaded into the Ansys software. In each element, the parameter was assigned that determines the value of Young's modulus and the ultimate stress according to (12), (13) (in Fig. 2 a grid with a color diagram indicating the distribution of the Young's modulus and the ultimate stress by volume is given). In Fig. 2, it can be seen that the cortical layer has the greatest stiffness and ultimate stress (red areas in the figure). It is worth commenting on the blue inclusions on the inner surface of the bone, which correspond to the small Young's modulus and the ultimate stress, this is due to the presence of pores. While scanning, we got weakened the integral value of the attenuation coefficient in a small region near pore.

After the solution, the stress distribution fields for the Mises and the safety factor calculated using the relation (14) were analyzed. Along with the inhomogeneous problem, the related homogeneous problem (having the same geometry, the same boundary conditions, but with volume averaged mechanical characteristics) was considered.

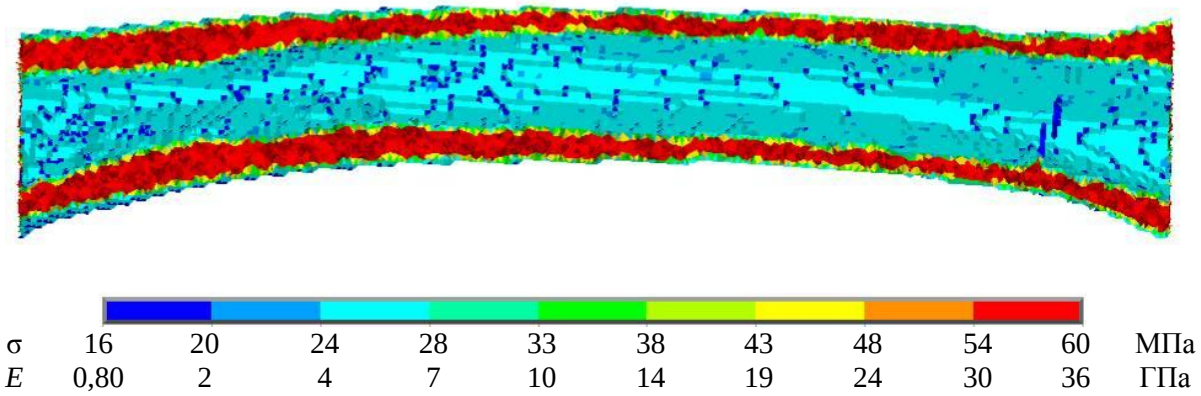

Fig. 2. Distribution of mechanical parameters the finite element model: the Young's modulus and ultimate stresses

Calculated case 1

For the case of sample compression, the localization of the maximum Mises stresses for a inhomogeneous sample occurred in the middle of the bone cortical lager at a distance of approximately one-third the length of the specimen from the termination (see Fig. 3, *a*). For a homogeneous sample, the localization of the maximum stresses by the Mises occurred on the outer surface of the cortical and moved insignificantly in the longitudinal direction to the loaded end (see Fig. 4, *a*). The numerical values of the maximum stresses in both cases differed not significantly: 36 and 37 MPa for the inhomogeneous and homogeneous sample, respectively. The margins of the factors of safety differed significantly.

In the case of a inhomogeneous sample, the factor of safety exceeded unity on the external and internal surfaces of the bone, in the region of localization of the maximum Mises stresses, while this region is extended: almost half of the sample (see Figs. 3, *b*, *c*), the largest value of the safety factor in this case was 1.38. For a homogeneous sample, the maximum value of the safety factor was reached in the same region where the maximum Mises stresses were located, the largest value of the safety factor in this case was 0.89 (see Figs. 4, *b*, *c*). That is, according to the inhomogeneous model, the sample will undergo destruction while, according to a homogeneous formulation of the critical values, the stresses are not attained. The difference in the safety factor was 55%.

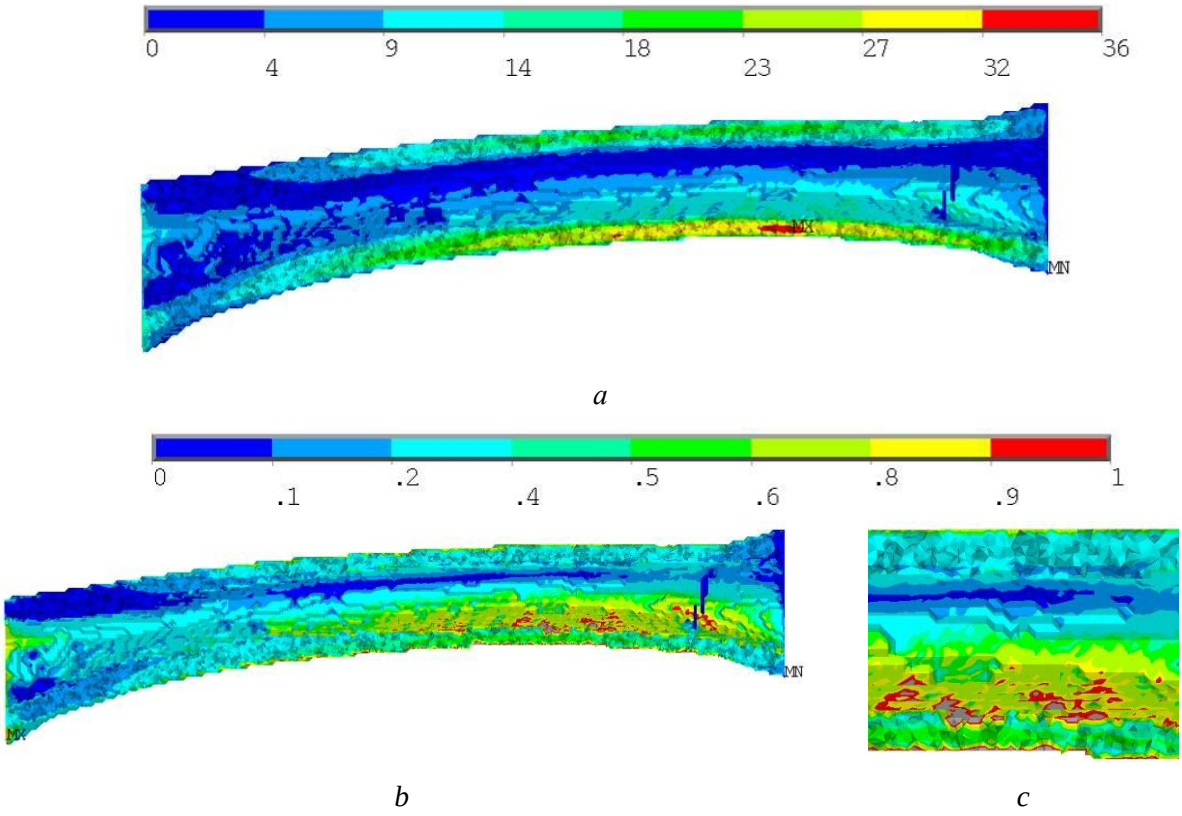

a

b *c*

Fig. 3. Results for the calculated case 1 of a inhomogeneous sample: *a* is distribution of Mises stresses, MPa; *b*, *c* is distribution of the factor of safety

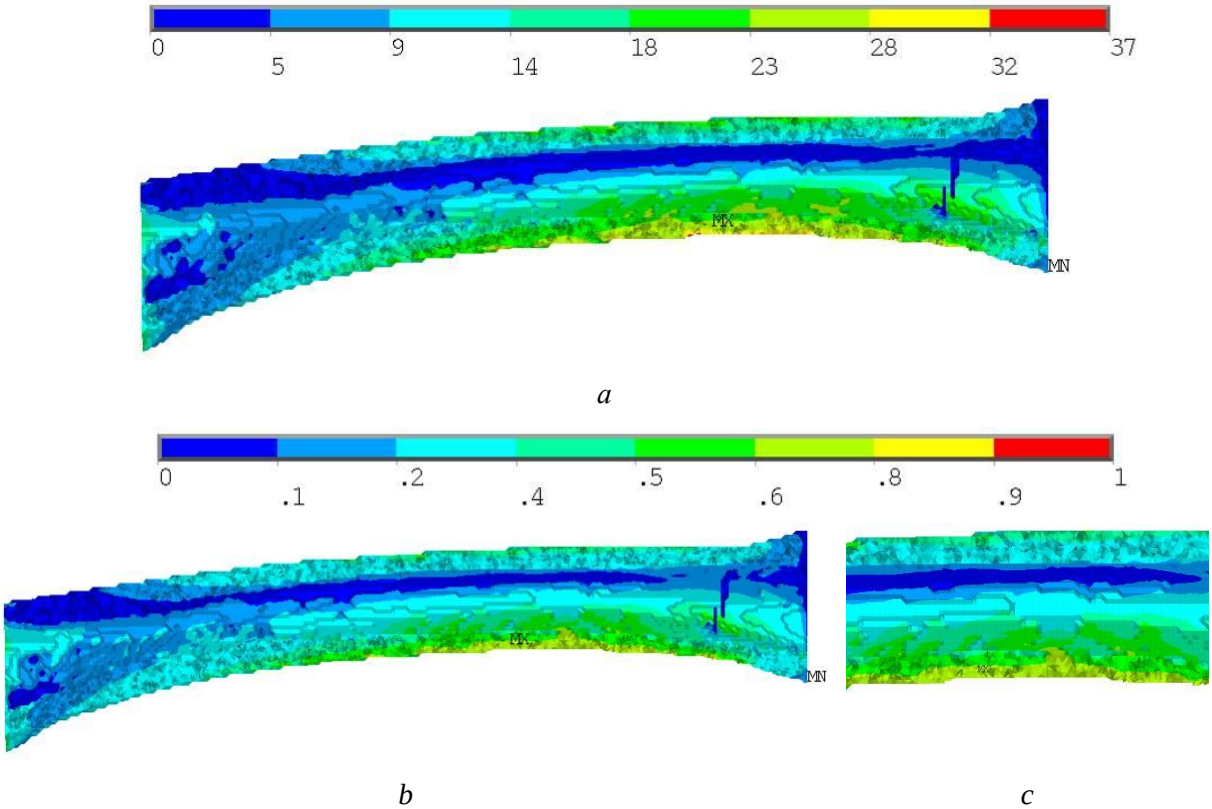

a

b *c*

Fig. 4. Results for the calculated case 1 of a homogeneous sample: *a* is distribution of Mises stresses, MPa; *b*, *c* is distribution of the factor of safety

Calculated case 2

For the case of sample bending, the localization of the maximum Mises stresses for a inhomogeneous sample occurred in the middle of the cortical bone at a small distance from the kinematic boundary condition (see Fig. 5, *a*). For a homogeneous sample, the localization of the maximum Mises stresses occurred on the outer surface of the cortical and approximately at the same distance from the kinematic boundary condition in the inhomogeneous case (see Fig. 6, *a*). Numerical values of maximum stresses in both cases differed not significantly: 24 and 23 MPa for a inhomogeneous and homogeneous sample, respectively. The differences in the distribution patterns of the factor of safety are similar to the first calculated case. In the case of a inhomogeneous sample, the factor of safety was close to the critical value (unity) on the outer and inner surfaces of the bone, in the region of localization of the maximum Mises stresses, this region significant (see Figs. 5, *b*, *c*), the largest value of the factor of safety in this case was 0.95. For the homogeneous sample, the maximum value of the factor of safety was reached in the same region where the maximum Mises stresses were located, the largest value of the safety factor in this case was 0.58 (see Figs. 6, *b*, *c*). That is, according to the inhomogeneous model, the sample will be close to fracture while, according to the homogeneous setting of the critical values, the stresses are not reached with sufficient margin. The difference in the factor of safety was 63%.

Calculated case 3

For the mutual case of the sample loading, the localization of the maximum Mises stresses for a inhomogeneous sample occurred in the middle of the bone cortical at a distance of approximately one-third the length of the specimen from the kinematic boundary conditions (see Figure 7, *a*). For a homogeneous sample, localization of the maximum Mises stresses occurred on the outer surface of the cortical and moved insignificantly in the longitudinal direction to the loaded end face (see Fig. 8, *a*). The numerical values of the maximum stresses in both cases differed not significantly: 57 and 53 MPa for the inhomogeneous and homogeneous sample, respectively. The margins of the factors of safety differed significantly. In the case of a inhomogeneous sample, the factor of safety exceeded unity on the external and internal surfaces of the bone, in the region of localization of the maximum Mises stresses, while this region is extended: almost half the sample and propagates along the circumferential direction (see Figs. 7, *b*, *c*), the largest value of the coefficient of the reserve in this case was 2.33. For a homogeneous sample, the maximum value of the factor of safety was reached in the same region where the maximum Mises stresses were localized - on the outer surface of the cortical, the largest value of the safety factor in this case was 1.28 (see Figs. 8, *b*, *c*). The difference in the safety factor was 82%. That is, under mutual loading, the sample will be destroyed at much lower strengths, according to the calculation of the inhomogeneous model, than calculations of the homogeneous model show. These examples illustrate the need to take into account the distribution of the mechanical properties of the bone organ when modelling the stress strain behavior . Patterns of distribution of the factor of safety are qualitatively changed, their quantitative values change significantly. The above method allows us to simulate the mechanical behavior of bone organs, taking into account the individualization of not only the geometry of the organ, but also its mechanical properties.

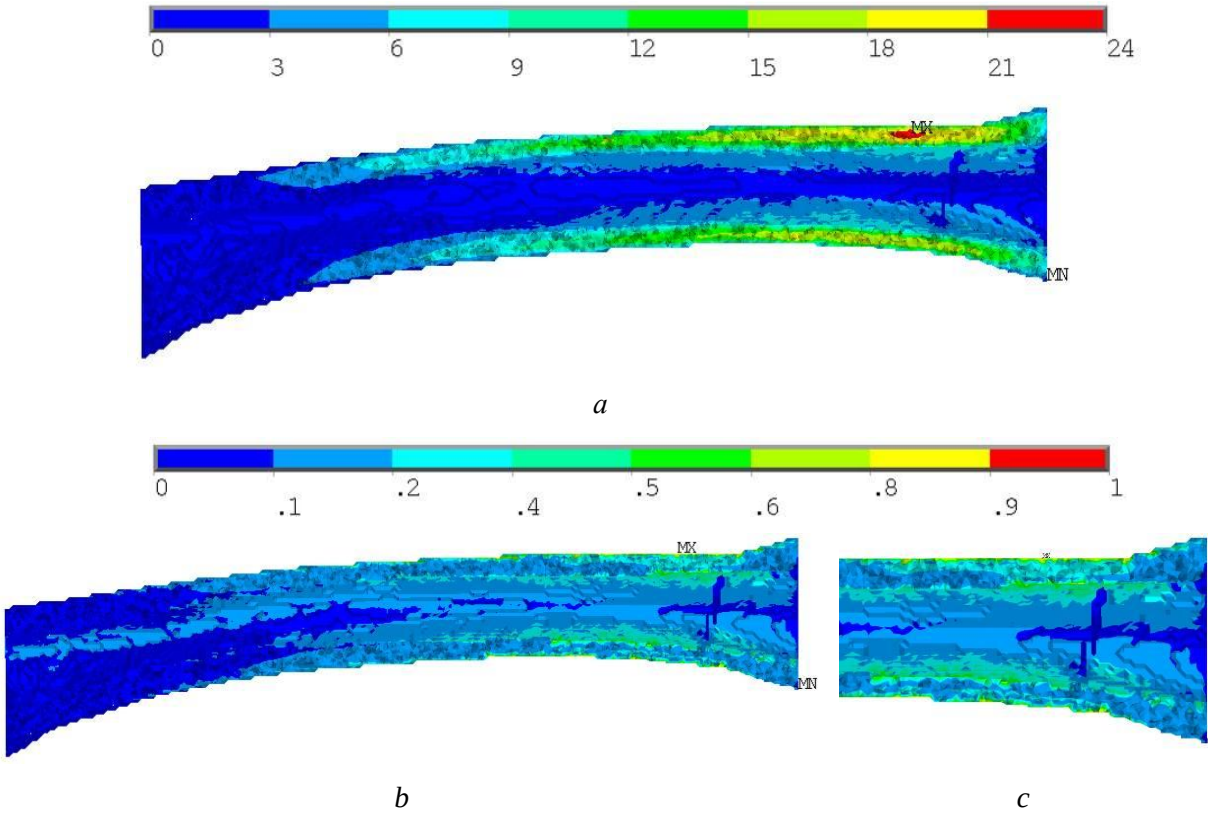

a

b *c*

Fig. 5. Results for the calculated case 2 of a inhomogeneous sample: *a* is distribution of Mises stresses, MPa; *b*, *c* is distribution of the factor of safety

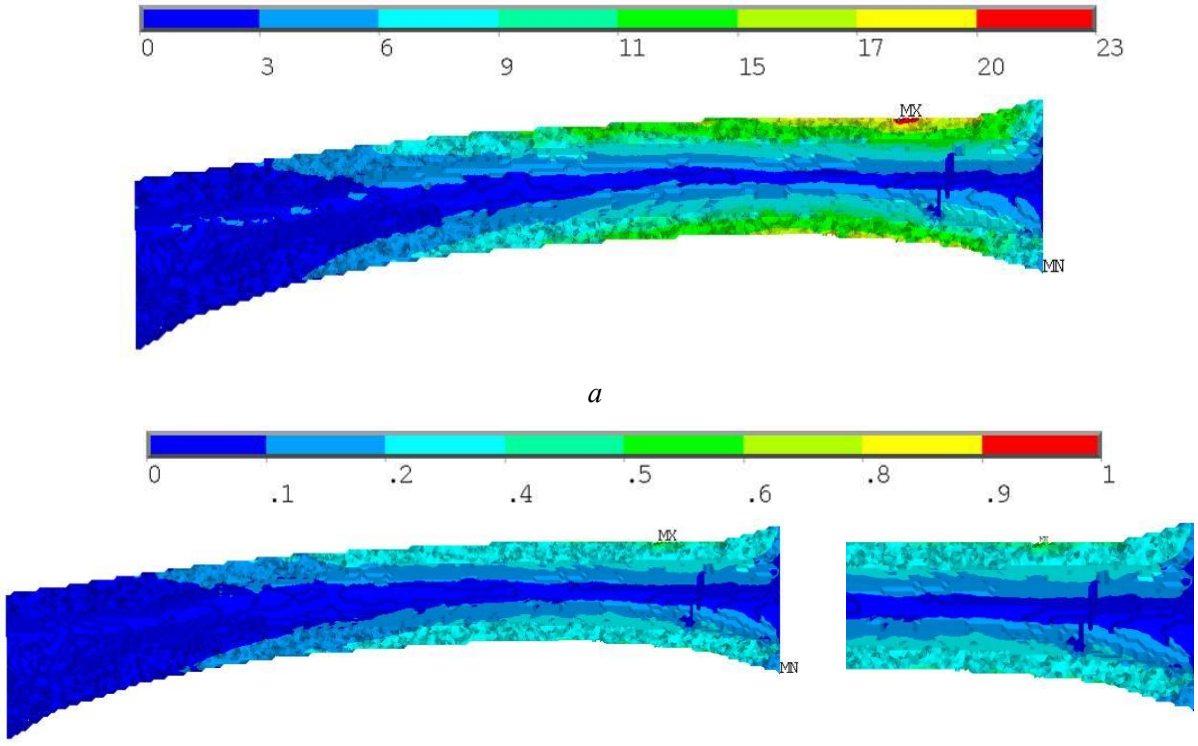

a

b *c*

Fig. 6. Results for the calculated case 2 of a homogeneous sample: *a* is distribution of Mises stresses, MPa; *b*, *c* is distribution of the factor of safety

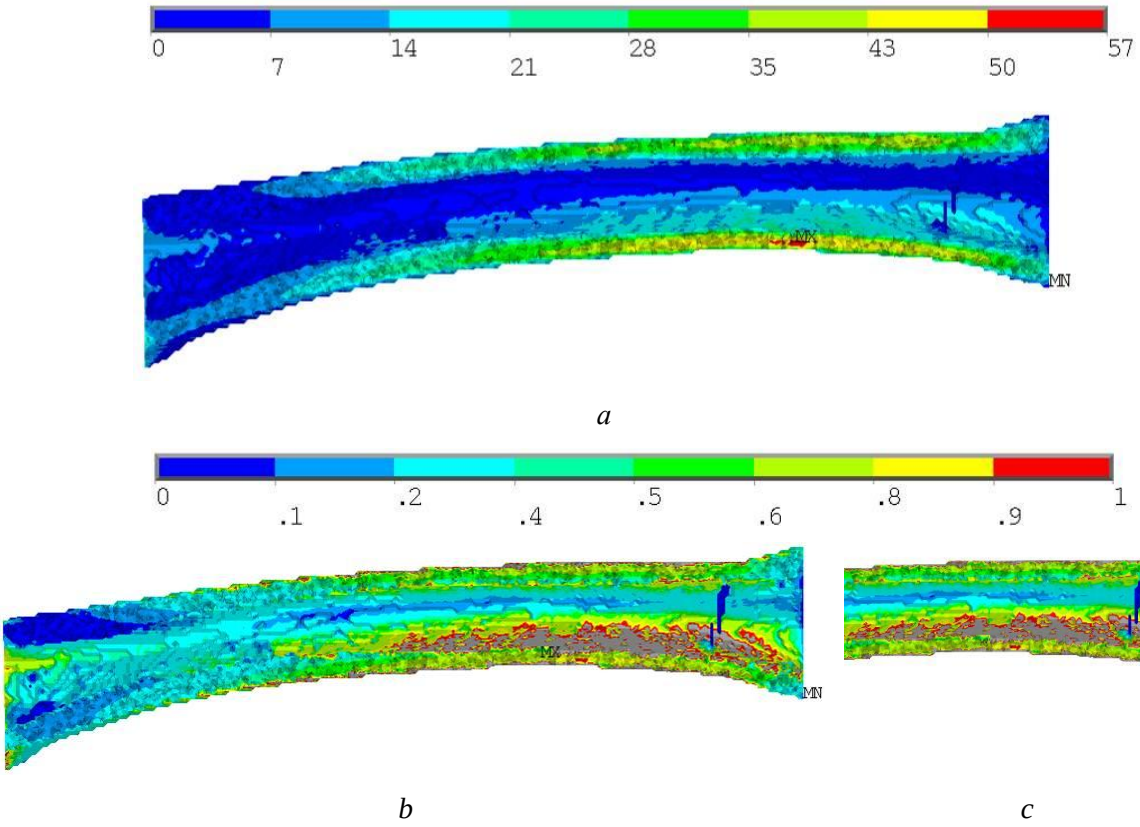

a

b *c*

Fig. 7. Results for the calculated case 3 of a inhomogeneous sample: *a* is distribution of Mises stresses, MPa; *b*, *c* is distribution of the factor of safety

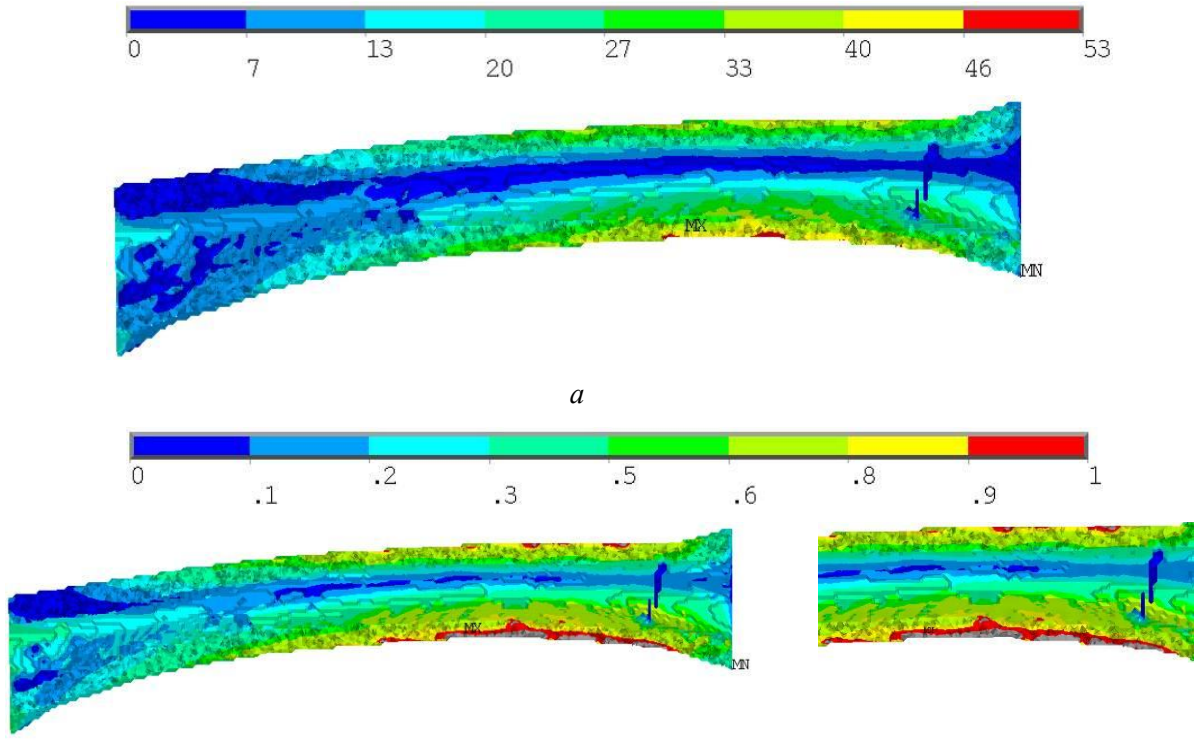

a

b *c*

Fig. 8. Results for the calculated case 3 of a homogeneous sample: *a* is distribution of Mises stresses, MPa; *b*, *c* is distribution of the factor of safety

CONCLUSIONS

1. In the work, a technique for constructing a finite-element inhomogeneous model of an organ from bone tissue according to computed tomography is presented.
2. Numerical results of model problems illustrate significant differences in the results of the stress-strain state of the organ and allow us to judge the local strength of bone tissue in terms of factor of safety.
3. In modeling, the following assumptions were made: the inhomogeneous material is isotropic, there is a relationship between physical density and mechanical characteristics, which allows us to use of optical density to calculate the Young's modulus and ultimate stress.
4. The application of the described technique allows us to use the factor of safety for analyze and making conclusion about the stress-strain state of the object under various external loads.
5. The proposed model can be expanded by taking into account the orthotropic nature of the material.

ACKNOWLEDGEMENTS

The work is partially supported by Russian Federation President Grant for Support of Young Scientists MK-1717.2018.1

Special thanks to Independent X-ray diagnostic centers «Picasso».

REFERENCES

1. Akulich A.Yu., Akulich Yu.V., Denisov A.S. The experimental fracture shear stress determination of the human femoral head spongy bone tissue. *Russian Journal of Biomechanics*, 2010, vol. 14, no. 4 (50), pp. 7-16
2. Akulich Yu.V., Akulich A.Yu., Denisov A.S. The influence of the number and sizes of thread fixators on the adaptive changes of the bone spongy tissue mechanical properties and bone fragment compression force after controlled osteosynthesis of the femoral neck fracture. *Russian Journal of Biomechanics*, 2012, vol. 16, no. 2 (56), pp. 17-24.
3. Akulich Yu.V., Akulich A.Yu., Denisov A.S., Shaymanov P.S., Shulyatev A.F. Correction of trabecular bone tissue individual relation between Young's modulus and volume bone fraction. *Russian Journal of Biomechanics*, 2014, vol. 18, no. 2, pp. 135-143
4. Akulich Yu.V., Podgayets R.M., Scryabin V.L., Sotin A.V. The investigation of stresses and strains in the hip joint after operation of endoprosthetics. *Russian Journal of Biomechanics*, 2007, vol. 11, no. 4, pp. 9-35.
5. Andreyev P.S., Konoplev Yu.G., Sachenkov O.A., Khasanov R.F., Yashina I.V. Matematicheskoye modelirovaniye rotatsionnoy fleksionnoy osteotomii [Mathematical modelling of rotational flexion osteotomy]. *Nauchno-tekhnicheskiy Vestnik Povolzhya*, 2014, no. 5, pp. 18-21 (*In Russian*).
6. Anisimov O.G., Akhtyamov I.F., Shigayev Ye.S. *Osobennosti statsionarnogo etapa lecheniya perelomov proksimalnogo otdela bedrennoy kosti* [Features of the Inpatient Treatment of Proximal Femur Fractures]. Kazan: *TaGraf*, 2017, 222 pp. (*In Russian*).
7. Akhtyamov I.F., Kovalenko A.N., Anisimov O.G., Zakirov R.Kh. Lecheniye osteonekroza golovki bedra [Treatment of Osteonecrosis of the Femoral Head]. *Skripta*, 2012, 176 p. (*In Russian*).
8. Akhtyamov I.F., Shakirova F.V., Klyushkina Yu.A., Baklanova D.A., Gatina E.B., Aliyev E.O. Experimental analysis of the healing process in the area of tibial bone fracture [Analysis of the regenerative process in the area of tibial fracture]. *Travmatologiya I Ortopediya Rossii*, 2016, no. 1(79), pp. 100-108 (*In Russian*).
9. Akhtyamov I.F., Khayertdinov I.S., Shigayev Ye.S., Kovalenko A.N., Gatina E.B. Lecheniye postradavshikh s perelomami proksimalnogo otdela bedrennoĭ kosti v usloviyakh Bol nitsy skoroĭ meditsinskoĭ pomoshchi [Treatment of patients with fractures of the proximal femur under the conditions of the emergency hospital]. *Sovremennoye Iskusstvo Meditsiny*, 2013, no.1(9), pp. 23-30 (*In Russian*).
10. Akhtyamov I.F., Shigayev Ye.S., Anisimov O.G *Osobennosti statsionarnogo etapa lecheniya perelomov proksimalnogo otdela bedrennoy kosti* [Features of the Inpatient Treatment of Proximal Femur Fractures]. Kazan, *TaGraf*, 2017, 222 pp. (*In Russian*).

11. Baltina T.V., Ahmetov N.F., Sachenkov O.A., Fedyanin A.O., Lavrov I.A. The influence of hindlimb unloading on bone and muscle tissues in rat model. *BioNanoSci*, 2017, 7(1), pp. 67-69. DOI: 10.1007/s12668-016-0288-8
12. Banetskiy M.V. *Biomekhanicheskoye obosnovaniye ispolzovaniya vertluzhnogo komponenta pri endoprotezirovanii tazobedrennogo sustava* [Biomechanical Justification for the Use of the Acetabular Component in Hip Joint Arthroplasty]. PhD Thesis, Moscow, 2008, 94 pp. (*In Russian*).
13. Beletskiy A.V., Akhtyamov I.F., Bogosyan A.B., Gerasimenko M.A. *Asepticheskiy nekroz golovki bedrennoy kosti u detey* [Aseptic Necrosis of the Femoral Head in Children]. *Skripta*, 2010, 255 p (*In Russian*).
14. Berezhnoy D.V., Sagdatullin M.K., Sultanov L.U. Raschet vzaimodeystviya deformiruyemykh konstruktsiy s uchetom treniya v zone kontakta na osnove metoda konechnykh elementov [Calculation of the interaction of deformable structures with friction in the contact zone based on the finite element method]. *Vestnik Kazanskogo tekhnologicheskogo universiteta*, 2014, vol. 17, no. 14, pp. 478-481 (*In Russian*).
15. Cuppone M., Seedhom B.B., Berry E., Ostell A.E. The longitudinal Young's modulus of cortical bone in the midshaft of human femur and its correlation with computer tomography scanning data. *Calcified Tissue International*, 2004, vol. 74(3), pp. 302–309.
16. Davydov R.L., Sultanov L.U. Numerical algorithm for investigating large elasto-plastic deformations. *Journal of Engineering Physics and Thermophysics*, 2015, vol. 88 (5), pp. 1280-1288. DOI: 10.1007/s10891-015-1310-7
17. Galiullin R.R., Sachenkov O.A., Khasanov R.F., Andreev P.S. Evalution of external fixation device stiffness for rotary osteotomy. *International Journal of Applied Engineering Research*, 2015, vol.10, no. 24, pp. 44855-44860.
18. Gupta S., Dan P. Bone geometry and mechanical properties of the human scapula using computed tomography data. *Trends Biomater. Artif. Organs*, 2004, vol. 17(2), pp. 61-70.
19. Heesakkers N., van Kempen R., Feith R., Hendriks J., Schreurs W. The long-term prognosis of Legg-Calvé-Perthes disease, a historical prospective study with a median follow-up of forty one years. *International Orthopaedics*, 2015, vol. 39 (5), pp. 859-863.
20. Ivanov D.V., Barabash A.P., Barabash Yu.A. New type of intramedullary nail for femur diaphyseal fracture osteosynthesis. *Russian Journal of Biomechanics*, 2012, vol. 19, no. 1, pp. 45-56.
21. Isaksson H., Malkiewicz M., Nowak R., Helminen H.J., Jurvelin J.S. Rabbit cortical bone tissue increases its elastic stiffness but becomes less viscoelastic with age. *Bone*, 2010, vol. 47(6), pp. 1030-1038.
22. Izmailova Z.T. Preoperative diagnostics of the modular transformation in the case of thigh bone transosseous osteosynthesis. *Russian Journal of Biomechanics*, 2009, vol. 13, no. 2(44), pp. 23-31.
23. Sachenkov O.A., Hasanov R.F., Andreev P.S., Konoplev Yu.G. Numerical study of stress-strain state of pelvis at the proximal femur rotation osteotomy. *Russian Journal of Biomechanics*, 2016, vol. 20, no. 3, pp. 220-232.
24. Kaneko T.S., Pejcic M.R., Tehranzadeh J., Keyak J.H. Relationships between material properties and computer tomographyscan data of cortical bone with and without metastatic lesions. *Med. Eng. Phys*, 2003, vol. 25(6), pp. 445-454.
25. Klimov O.V. Calculation and control of biomechanical axis of the lower limbs in frontal plane at its correction according to Ilizarov. *Russian Journal of Biomechanics*, 2014, vol. 18, no. 2, pp. 209-216.
26. Menshchikova T.I., Dolganova T.I., Aranovich A.M. The effect of femur and leg muscle strength on foot support responses in patients with achondroplasia after height correction. *Russian Journal of Biomechanics*, 2014, vol. 18, no. 2, pp. 217-225.
27. Nakamura N., Inaba Y., Machida J., Saito T. Rotational open-wedge osteotomy improves treatment outcomes for patients older than eight years with Legg-Calve-Perthes disease in the modified lateral pillar B/C border or C group. *International Orthopaedics*, 2015, vol. 39 (7), pp. 1359-1364.
28. Ozel B.D., Ozel D., Ozkan F., Halefoglu A.M. Diffusion-weighted magnetic resonance imaging of femoral head osteonecrosis in two groups of patients, Legg-Perthes-Calve and Avascular necrosis. *Radiologia Medica*, 2016, vol. 121 (3), pp. 206-213.
29. Pailhe R., Cavaignac E., Murgier J., de Gauzy J.S., Accadbled F. Triple osteotomy of the pelvis for Legg-Calve-Perthes disease, a mean fifteen year follow-up. *International Orthopaedics*, 2016, vol. 40 (1), pp. 115-122.
30. Rho J.Y., Hobatho M.C., Ashman R.B. Relations of mechanical properties to density and computer tomographynumbers in human bone. *Med. Eng. Phys*, 1995, vol. 17(5), pp. 347-55.
31. Sachenkov O., Kharislamova L., Shamsutdinova N., Kirillova E. and Konoplev Yu. Evaluation of the bone tissue mechanical parameters after induced alimentary Cu-deficiency followed by supplementary injection of Cu nanoparticles in rats. *IOP Conference Series, Materials Science and Engineering*, 2015, vol. 98, 012015. DOI: 10.1088/1757-899X/98/1/012015
32. Shilko S.V., Chernous D.A., Bondarenko K.K. A method for in vivo estimation of viscoelastic characteristics of skeletal muscles. *Russian Journal of Biomechanics*, 2007, vol. 11, no. 1, pp. 44-53.

33. Shigapova F.A., Baltina T.V., Konoplev Y.G., Sachenkov O.A. Methods for automatic processing and analysis of orthotropic biological structures by microscopy and computed. *International Journal of Pharmacy & Technology*, 2016, vol. 8, no. 3, pp. 14953-14964.
34. Sagdatullin M.K., Berezhnoi D.V. Statement of the problem of numerical modelling of finite deformations. *Applied Mathematical Sciences*, 2014, vol. 8, no. 35, pp. 1731-1738. DOI: 12988/ams. 2014.4283
35. Tverier V.M., Nikitin V.N. The problem of occlusion correction in the human maxillofacial system. *Russian Journal of Biomechanics*, 2015, vol. 19, no. 4, pp. 296-308.
36. Tverier V.M., Nyashin Y.I., Nikitin V.N. Biomechanical model of determination of muscle and ligament forces in the human maxillofacial system. *Russian Journal of Biomechanics*, 2013, vol. 17, no. 2(60), pp. 5-15.

Received 5 September 2018